arXiv:hep-ex/0512029 v1 13 Dec 2005

Measurement of the J/ψ Production Cross Section in 920 GeV/c Fixed-Target Proton-Nucleus Interactions

HERA-B Collaboration

I. Abt[23], M. Adams[10], M. Agari[13], H. Albrecht[12], A. Aleksandrov[29], V. Amaral[8], A. Amorim[8], S. J. Aplin[12], V. Aushev[16], Y. Bagaturia[12,36], V. Balagura[22], M. Bargiotti[6], O. Barsukova[11], J. Bastos[8], J. Batista[8], C. Bauer[13], Th. S. Bauer[1], A. Belkov[11,†], Ar. Belkov[11], I. Belotelov[11], A. Bertin[6], B. Bobchenko[22], M. Böcker[26], A. Bogatyrev[22], G. Bohm[29], M. Bräuer[13], M. Bruinsma[28,1], M. Bruschi[6], P. Buchholz[26], T. Buran[24], J. Carvalho[8], P. Conde[2,12], C. Cruse[10], M. Dam[9], K. M. Danielsen[24], M. Danilov[22], S. De Castro[6], H. Deppe[14], X. Dong[3], H. B. Dreis[14], V. Egorytchev[12], K. Ehret[10], F. Eisele[14], D. Emeliyanov[12], S. Essenov[22], L. Fabbri[6], P. Faccioli[6], M. Feuerstack-Raible[14], J. Flammer[12], B. Fominykh[22], M. Funcke[10], Ll. Garrido[2], A. Gellrich[29], B. Giacobbe[6], J. Gläß[20], D. Goloubkov[12,33], Y. Golubkov[12,34], A. Golutvin[22], I. Golutvin[11], I. Gorbounov[12,26], A. Gorišek[17], O. Gouchtchine[22], D. C. Goulart[7], S. Gradl[14], W. Gradl[14], F. Grimaldi[6], Yu. Guilitsky[22,35], J. D. Hansen[9], J. M. Hernández[29], W. Hofmann[13], M. Hohlmann[12], T. Hott[14], W. Hulsbergen[1], U. Husemann[26], O. Igonkina[22], M. Ispiryan[15], T. Jagla[13], C. Jiang[3], H. Kapitza[12], S. Karabekyan[25], N. Karpenko[11], S. Keller[26], J. Kessler[14], F. Khasanov[22], Yu. Kiryushin[11], I. Kisel[23], E. Klinkby[9], K. T. Knöpfle[13], H. Kolanoski[5], S. Korpar[21,17], C. Krauss[14], P. Kreuzer[12,19], P. Križan[18,17], D. Krücker[5], S. Kupper[17], T. Kvaratskheliia[22], A. Lanyov[11], K. Lau[15], B. Lewendel[12], T. Lohse[5], B. Lomonosov[12,32], R. Männer[20], R. Mankel[29], S. Masciocchi[12], I. Massa[6], I. Matchikhilian[22], G. Medin[5], M. Medinnis[12], M. Mevius[12], A. Michetti[12], Yu. Mikhailov[22,35], R. Mizuk[22], R. Muresan[9], M. zur Nedden[5], M. Negodaev[12,32], M. Nörenberg[12], S. Nowak[29], M. T. Núñez Pardo de Vera[12], M. Ouchrif[28,1], F. Ould-Saada[24], C. Padilla[12], D. Peralta[2], R. Pernack[25], R. Pestotnik[17], B. AA. Petersen[9], M. Piccinini[6], M. A. Pleier[13], M. Poli[6,31], V. Popov[22], D. Pose[11,14], S. Prystupa[16], V. Pugatch[16], Y. Pylypchenko[24], J. Pyrlik[15], K. Reeves[13], D. Reßing[12], H. Rick[14], I. Riu[12], P. Robmann[30], I. Rostovtseva[22], V. Rybnikov[12], F. Sánchez[13], A. Sbrizzi[1], M. Schmelling[13], B. Schmidt[12], A. Schreiner[29], H. Schröder[25], U. Schwanke[29], A. J. Schwartz[7], A. S. Schwarz[12], B. Schwenninger[10], B. Schwingenheuer[13], F. Sciacca[13], N. Semprini-Cesari[6], S. Shuvalov[22,5], L. Silva[8], L. Sözüer[12], S. Solunin[11], A. Somov[12], S. Somov[12,33], J. Spengler[13], R. Spighi[6], A. Spiridonov[29,22], A. Stanovnik[18,17], M. Starič[17], C. Stegmann[5], H. S. Subramania[15],

M. Symalla[12,10], I. Tikhomirov[22], M. Titov[22], I. Tsakov[27], U. Uwer[14], C. van Eldik[12,10], Yu. Vassiliev[16], M. Villa[6], A. Vitale[6], I. Vukotic[5,29], H. Wahlberg[28], A. H. Walenta[26], M. Walter[29], J. J. Wang[4], D. Wegener[10], U. Werthenbach[26], H. Wolters[8], R. Wurth[12], A. Wurz[20], Yu. Zaitsev[22], M. Zavertyaev[12,13,32], T. Zeuner[12,26], A. Zhelezov[22], Z. Zheng[3], R. Zimmermann[25], T. Živko[17], A. Zoccoli[6]

[1] *NIKHEF, 1009 DB Amsterdam, The Netherlands* [a]
[2] *Department ECM, Faculty of Physics, University of Barcelona, E-08028 Barcelona, Spain* [b]
[3] *Institute for High Energy Physics, Beijing 100039, P.R. China*
[4] *Institute of Engineering Physics, Tsinghua University, Beijing 100084, P.R. China*
[5] *Institut für Physik, Humboldt-Universität zu Berlin, D-12489 Berlin, Germany* [c,d]
[6] *Dipartimento di Fisica dell' Università di Bologna and INFN Sezione di Bologna, I-40126 Bologna, Italy*
[7] *Department of Physics, University of Cincinnati, Cincinnati, Ohio 45221, USA* [e]
[8] *LIP Coimbra, P-3004-516 Coimbra, Portugal* [f]
[9] *Niels Bohr Institutet, DK 2100 Copenhagen, Denmark* [g]
[10] *Institut für Physik, Universität Dortmund, D-44221 Dortmund, Germany* [d]
[11] *Joint Institute for Nuclear Research Dubna, 141980 Dubna, Moscow region, Russia*
[12] *DESY, D-22603 Hamburg, Germany*
[13] *Max-Planck-Institut für Kernphysik, D-69117 Heidelberg, Germany* [d]
[14] *Physikalisches Institut, Universität Heidelberg, D-69120 Heidelberg, Germany* [d]
[15] *Department of Physics, University of Houston, Houston, TX 77204, USA* [e]
[16] *Institute for Nuclear Research, Ukrainian Academy of Science, 03680 Kiev, Ukraine* [h]
[17] *J. Stefan Institute, 1001 Ljubljana, Slovenia* [i]
[18] *University of Ljubljana, 1001 Ljubljana, Slovenia*
[19] *University of California, Los Angeles, CA 90024, USA* [j]
[20] *Lehrstuhl für Informatik V, Universität Mannheim, D-68131 Mannheim, Germany*
[21] *University of Maribor, 2000 Maribor, Slovenia*
[22] *Institute of Theoretical and Experimental Physics, 117259 Moscow, Russia* [k]
[23] *Max-Planck-Institut für Physik, Werner-Heisenberg-Institut, D-80805 München, Germany* [d]
[24] *Dept. of Physics, University of Oslo, N-0316 Oslo, Norway* [l]
[25] *Fachbereich Physik, Universität Rostock, D-18051 Rostock, Germany* [d]
[26] *Fachbereich Physik, Universität Siegen, D-57068 Siegen, Germany* [d]

[27] *Institute for Nuclear Research, INRNE-BAS, Sofia, Bulgaria*
[28] *Universiteit Utrecht/NIKHEF, 3584 CB Utrecht, The Netherlands* [a]
[29] *DESY, D-15738 Zeuthen, Germany*
[30] *Physik-Institut, Universität Zürich, CH-8057 Zürich, Switzerland* [m]
[31] *visitor from Dipartimento di Energetica dell' Università di Firenze and INFN Sezione di Bologna, Italy*
[32] *visitor from P.N. Lebedev Physical Institute, 117924 Moscow B-333, Russia*
[33] *visitor from Moscow Physical Engineering Institute, 115409 Moscow, Russia*
[34] *visitor from Moscow State University, 119899 Moscow, Russia*
[35] *visitor from Institute for High Energy Physics, Protvino, Russia*
[36] *visitor from High Energy Physics Institute, 380086 Tbilisi, Georgia*
[†] *deceased*

[a] supported by the Foundation for Fundamental Research on Matter (FOM), 3502 GA Utrecht, The Netherlands
[b] supported by the CICYT contract AEN99-0483
[c] supported by the German Research Foundation, Graduate College GRK 271/3
[d] supported by the Bundesministerium für Bildung und Forschung, FRG, under contract numbers 05-7BU35I, 05-7DO55P, 05-HB1HRA, 05-HB1KHA, 05-HB1PEA, 05-HB1PSA, 05-HB1VHA, 05-HB9HRA, 05-7HD15I, 05-7MP25I, 05-7SI75I
[e] supported by the U.S. Department of Energy (DOE)
[f] supported by the Portuguese Fundação para a Ciência e Tecnologia under the program POCTI
[g] supported by the Danish Natural Science Research Council
[h] supported by the National Academy of Science and the Ministry of Education and Science of Ukraine
[i] supported by the Ministry of Education, Science and Sport of the Republic of Slovenia under contracts number P1-135 and J1-6584-0106
[j] supported by the U.S. National Science Foundation Grant PHY-9986703
[k] supported by the Russian Ministry of Education and Science, grant SS-1722.2003.2, and the BMBF via the Max Planck Research Award
[l] supported by the Norwegian Research Council
[m] supported by the Swiss National Science Foundation

Abstract

The mid-rapidity ($d\sigma_{pN}/dy$ at y=0) and total (σ_{pN}) production cross sections of J/ψ mesons are measured in proton-nucleus interactions. Data collected by the HERA-B experiment in interactions of 920 GeV/c protons with carbon, titanium and tungsten targets are used for this analysis. The J/ψ mesons are reconstructed by their decay into lepton pairs. The total production cross section obtained is

$\sigma_{pN}^{J/\psi} = 663 \pm 74 \pm 46$ nb/nucleon. In addition, our result is compared with previous measurements.

PACS: 13.20Gd, 13.85Ni, 24.85+p

1 Introduction

Since the spectacular discovery of the J/ψ particle [1,2] heavy-quarkonium production in hadron-hadron interactions has been in the focus of interest because it provides important information on both perturbative and non-perturbative aspects of Quantum Chromodynamics (QCD). Especially the unexpectedly large cross sections for J/ψ and $\psi(2S)$ at large transverse momenta observed by the CDF experiment [3] renewed this interest and led to the development of the non-relativistic QCD (NRQCD) approach [4], which extends the color-singlet model by including color-octet contributions [5,6,7]. A different approach to charmonium production is based on the color evaporation model [8,9]. Both models predict the energy dependence of J/ψ production.

These theoretical predictions have to be compared to the experimental results obtained in proton induced reactions. However, despite the large interest in this field, the experimental situation is far from being satisfactory. Cross section measurements at comparable energies differ well outside the quoted uncertainties. Thus a new measurement with low systematic errors is of interest.

In this paper, we report on a measurement of the cross section for J/ψ production in interactions of 920 GeV/c protons with nuclei of atomic weight A using the HERA-B detector. The corresponding center of mass energy of the proton nucleon interaction is $\sqrt{s}$=41.6 GeV. A data sample of 210 million interactions on carbon, titanium and tungsten targets was recorded using a minimum bias trigger in the 2002-2003 HERA running period. The J/ψ mesons are detected in the inclusive reaction

$$pA \rightarrow \; J/\psi \; X \text{ with } J/\psi \; \rightarrow \; e^+e^- \text{ or } \mu^+\mu^- \; .$$

The advantage of such a minimum bias data sample is the low systematic error due to the large ($> 97\%$) trigger efficiency, the large angular coverage of HERA-B and its large reconstruction efficiency. On the other hand, the size of the sample is small, since charmonium cross sections are $4 - 5$ orders of magnitude less than the total inelastic cross section.

2 Apparatus

The HERA-B fixed-target spectrometer operated at the 920 GeV/c proton beam of the HERA storage ring at DESY using one or more wire targets inserted into the beam halo. The detector was equipped with a vertex detector and extensive tracking and particle identification systems. It had a large geometrical coverage from 15 mrad to 220 mrad in the bending (horizontal) plane and 15 mrad to 160 mrad in the non-bending (vertical) plane. Fig. 1 shows a plan view of the detector in the configuration of the 2002-2003 data run.

The target system [10] consisted of two stations of four wires each. The wires were positioned above, below, and on either side of the beam and were made from various materials including carbon, titanium and tungsten. The stations were separated by 40 mm along the beam direction. The wires were positioned individually in the halo of the stored proton beam and the interaction rate for each inserted wire was adjusted independently.

The Vertex Detector System (VDS) [11] was a forward micro-strip vertex detector integrated into the HERA proton ring. It provided a precise measurement of primary and secondary vertices. The VDS consisted of 7 stations (with 4 stereo views each) of double-sided silicon strip detectors (50×70 mm, 50 μm pitch) integrated into a Roman pot system inside a vacuum vessel and operated as near as 10 mm from the beam. An additional station was mounted immediately downstream of the 3 mm thick aluminum window of the vacuum vessel.

The first station of the main tracker was placed upstream of the 2.13 Tm spectrometer dipole magnet. The remaining 6 tracking stations extended from the downstream end of the magnet to the electromagnetic calorimeter (ECAL) located 13 m downstream of the target. Each tracking station was divided into inner and outer detectors. The region starting from the beam pipe and extending up to 200 mm was covered by micro-strip gas chambers with GEM foils (inner tracker [12]) which, however, were not used in this analysis due to insufficient stability. The region outside the inner tracker was covered by the large area outer tracker (OTR) [13] consisting of $\approx$95,000 channels of honeycomb drift cells.

Particle identification was performed by a Ring Imaging Cherenkov detector (RICH) [14], an electromagnetic calorimeter (ECAL) [15] and a muon detector (MUON) [16]. The RICH used C_4F_{10} as radiator gas and two large spherical mirrors to project Cherenkov photons on the photon detector employing multi-anode photomultipliers. The ECAL was based on "shashlik" sampling calorimeter technology, consisting of scintillator layers sandwiched between metal absorbers. It was subdivided in three different sections with

increasing cell size. In the radially innermost section, tungsten was used as an absorber, and lead was used everywhere else. The MUON detector was segmented into four super-layers. Iron and concrete shielding extended from just behind the ECAL to the last MUON super-layer, except for gaps for the super-layers themselves. The first two super-layers consisted of three layers of tube chambers with different stereo angles. The last two super-layers each consisted of one layer of tube chambers with additional cathode pad readout.

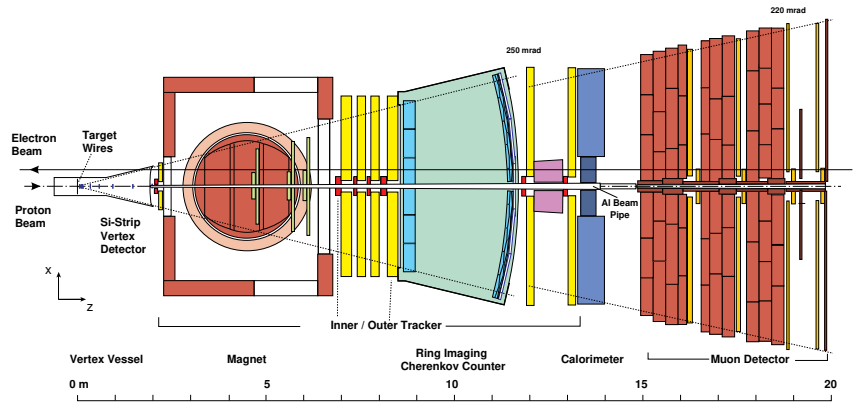

Figure 1. Plan view (bending plane) of the HERA-B detector.

3 Data Sample and Trigger

The present analysis is performed on single wire carbon, titanium and tungsten runs taken under stable conditions with a minimum bias trigger with a total of 182 million interactions (Table 1). The trigger required at least 20 hits in the RICH detector (compared to an average of 33 for a full ring from a $\beta = 1$ particle [14]) or an energy deposit of at least 1 GeV in the electromagnetic calorimeter and was sensitive to $\epsilon_{trigger} > 97\%$ of the total inelastic cross section σ_{inel}.

The integrated luminosity was determined [17] from the number of inelastic interactions N_{inel} using the expression $\mathcal{L} = N_{inel}/(\epsilon_{trigger} \cdot \sigma_{inel})$. The data were recorded at a moderate interaction rate of about 1.5 MHz which corresponds to 0.17 interactions per filled bunch crossing. Therefore only about 10% of the events contain more than one interaction. The high data acquisition rate of about 1000 Hz allowed to record the bulk of the data within two weeks.

The information delivered by the vertex detector, outer tracker, electromagnetic calorimeter and muon detector entered into this analysis.

Target	Events	$\mathcal{L}(\mu b^{-1})$	$\Delta(\mathcal{L})/\mathcal{L}$
C Below 1	68.8 M	277.	4.8%
C Inner 2	20.5 M	98.0	4.8%
Ti Below 2	24.7 M	30.9	5.0%
W Inner 1	67.6 M	35.7	3.8%

Table 1
Summary of minimum bias statistics. Target material, wire position with respect to the proton beam (inner wire corresponds to +X and outer wire to -X, see Fig. 1), integrated luminosities as well as the sample-specific luminosity errors are given. In addition, a 2.0% scaling error on luminosity has to be taken into account.

4 Data Analysis

4.1 Event Selection

The search for J/ψ candidates is performed by analyzing the invariant mass spectrum of unlike-sign lepton pairs. The phase-space region of the J/ψ, in rapidity y, covered by our measurement is $-1.25 < y < +0.35$. The corresponding range in Feynman x_F is $-0.225 < x_F < +0.075$. Throughout this paper, the rapidity is defined in the proton-nucleon center-of-mass system. Soft cuts (see Table 2) are applied on the number of hits in the tracking system to select properly reconstructed tracks. Cutting on the dilepton vertex fit probability ensures that the two tracks have a common vertex. A cut on the transverse momentum of the leptons helps to reduce the background with a small loss ($< 3\%$) in signal efficiency.

The signal to background ratio can be improved by applying more stringent cuts on the lepton identification. In order to find the best set of cut values the signal significance $S/\sqrt{S+B}$ is maximized. S is the number of J/ψ surviving the selection cuts in the J/ψ Monte Carlo sample (see Sec. 5) scaled to obtain a comparable number of reconstructed J/ψ in Monte Carlo as in real data. The background B is evaluated from the like sign invariant mass spectrum in a 2.5 standard deviation window around the J/ψ position. Such a procedure allows to adjust the lepton identification criteria in an unbiased way.

Muon candidates are selected by requiring that the muon likelihood L_μ (normalized to one) derived from the muon hit information is greater than 0.2.

In the case of electrons, the background is higher due to pions interacting in the ECAL and charged hadrons overlapping with energy depositions by neutral particles. We therefore require that the track position extrapolated

	$\mu^+\mu^-$	e^+e^-
Number of hits in VDS (12 hits on average)	≥ 6	
Number of hits in OTR (40 hits on average)	≥ 10	
Transverse mom. p_T (GeV/c)	> 0.7	
Dilepton rapidity	$-1.25 < y < +0.35$	
Dilepton vertex fit probability	$> 10^{-5}$	
Muon likelihood (L_μ)	> 0.2	
VDS-ECAL match		$\|\Delta Y\| < 0.75$ cell width
E/p		$-2.0 < (E/p - 0.98)/\sigma < +3.5$

Table 2
Event selection requirements. The lepton identification cuts (last three rows) are fixed by the optimization procedure described in the text.

to the ECAL in the non-bending direction Y matches a cluster with $|\Delta Y| < 0.75$ cell width. Moreover, the ratio E/p, where E is the energy deposited in the electromagnetic calorimeter and p the momentum measured by the tracking system, provides good discrimination between electrons and hadrons. However, the electrons can emit Bremsstrahlung photons (BR) when passing the detector planes. BR photons emitted before the magnet are searched for in the ECAL and the momentum of the electron is corrected if such a cluster is found. Details of this procedure are explained in [18].

Additional energy losses result in a small deviation of the ratio E/p from unity. Consequently, a track is identified as an electron candidate if $-2.0 < (E/p - 0.98)/\sigma < +3.5$ with $\sigma \approx 6\%$.

4.2 $J/\psi \to \mu^+\mu^-$

The dimuon invariant mass distribution that results from combining all data-sets and applying the selection criteria discussed above is plotted in Fig. 2a. This distribution is fitted by a Gaussian plus a tail in the signal region and an exponential for the background. The tail takes into account the radiative process $J/\psi \to \mu^+\mu^-\gamma$ [19] whereas the background shape is suggested by the mass spectrum of like-sign lepton pairs (see Fig. 2b).

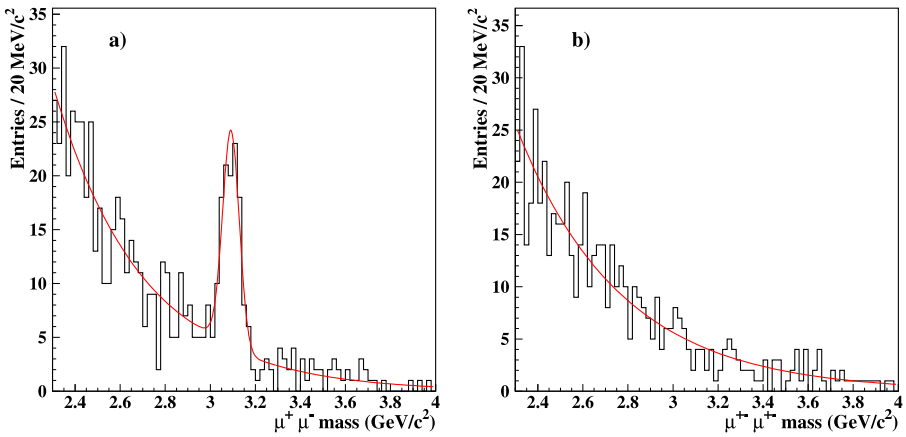

Figure 2. a) Unlike sign pairs fitted with a Gaussian plus a radiative tail for the signal and an exponential for the background; b) like sign dimuon candidates fitted with an exponential.

A fit with this function results in 100 ± 12 $J/\psi \to \mu^+\mu^-$ decays. To indicate the influence of the radiative tail, the mass distribution is fitted with a simple Gaussian resulting in 94 ± 12 events.

The peak position and the width (FWHM) are 3.093 ± 0.005 GeV/c^2 and 85 ± 10 MeV/c^2, respectively. The width is in good agreement with the width expected from the J/ψ Monte Carlo simulation (see Sec. 5). These fit results are used as input to the fit of the individual signals obtained from the three different data samples shown in Fig. 3a-c. The sum of the three signals (see Table 3) is in good agreement with the fit to the total sample.

$J/\psi \to \mu^+\mu^-$	total sample	subsample
Fit including radiative tail	100±12	
carbon		25±6
titanium		16±4
tungsten		58±9
$J/\psi \to e^+e^-$	total sample	subsample
Fit including radiative tail	57±13	
carbon		32±8
titanium		2±4
tungsten		24±10

Table 3
Signal yield for $J/\psi \to \mu^+\mu^-$ and $J/\psi \to e^+e^-$.

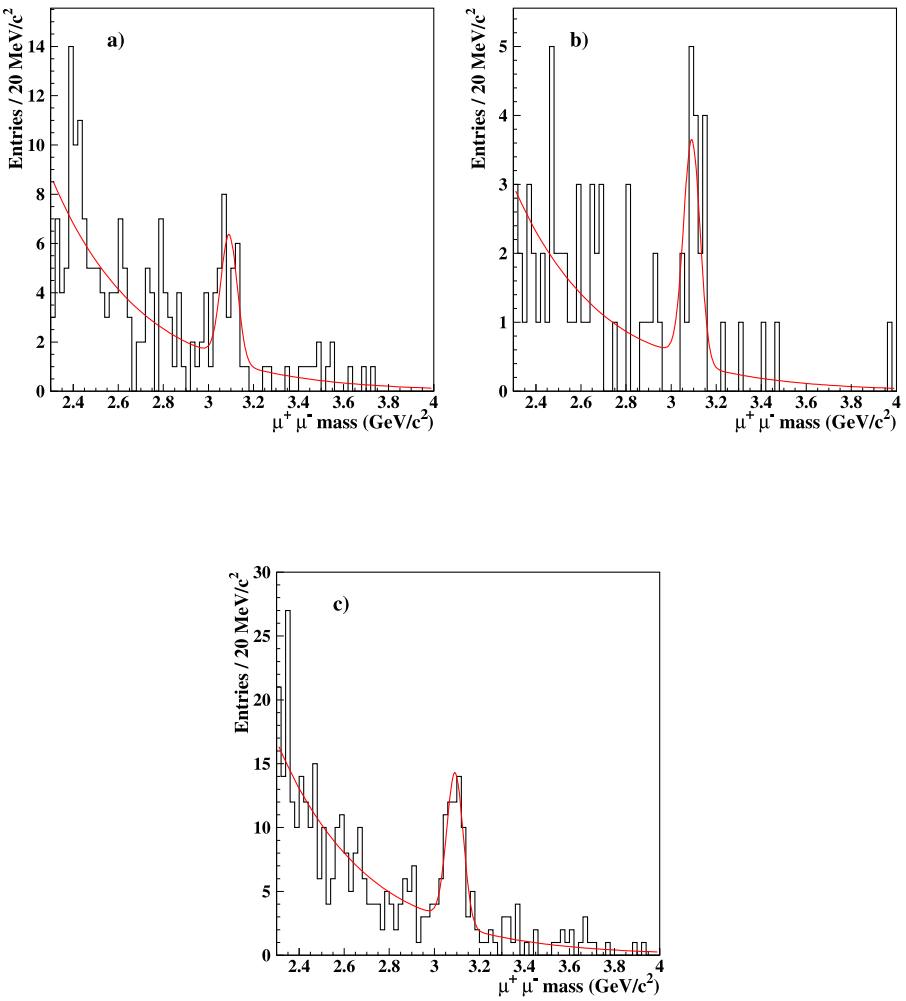

Figure 3. Invariant mass of unlike sign muon pairs from a) carbon, b) titanium, and c) tungsten sample.

4.3 $J/\psi \to e^+e^-$

In contrast to muons, the momentum measurement of electrons is distorted by energy losses due to the emission of Bremsstrahlung in the detector planes before the electromagnetic calorimeter. Consequently, the dielectron mass distribution shows a more pronounced tail towards smaller masses. The description of this tail taking into account Bremsstrahlung losses as well as the radiative tail due to the decay $J/\psi \to e^+e^-\gamma$ was adjusted by using our dilepton-triggered $J/\psi \to e^+e^-$ sample [20] which was recorded in the same data taking period with the same detector set-up. Fig. 4a displays the dielectron invariant mass distribution after applying the selection criteria listed in Table 2. Using an exponential to describe the background we obtain 57 ± 13 $J/\psi \to e^+e^-$ events (Table 3). As for the muons, the exponential background can be motivated by the like sign mass spectrum shown in Fig. 4b.

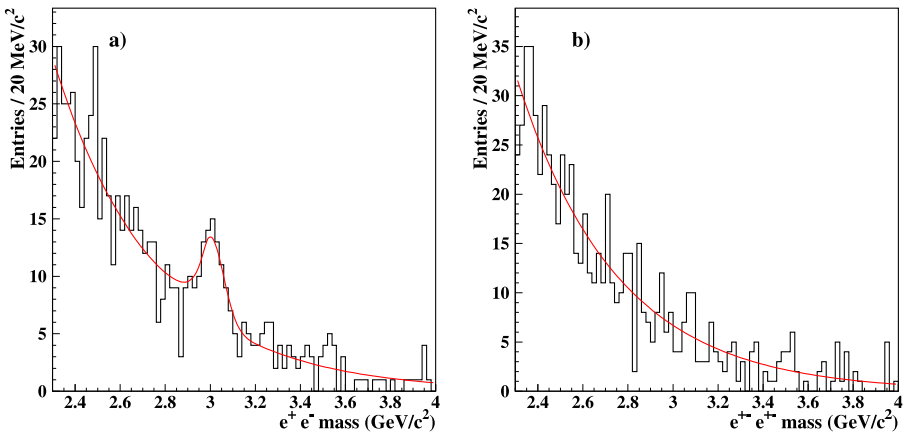

Figure 4. a) Invariant mass of unlike sign electron pairs fitted with a Gaussian plus a radiative tail for the signal and an exponential for the background; b) like sign dielectron candidates fitted with an exponential.

5 Efficiency Determination

A Monte Carlo simulation is used to determine the $J/\psi \to \ell^+\ell^-$ efficiencies. The Monte Carlo samples for $pA \to J/\psi + X$ are generated in two steps. First, a $c\bar{c}$ pair is generated with PYTHIA 5.7 [21] such that a J/ψ is always produced. The generated events are reweighted such that the resulting cross sections conform to the parameterizations

$$\frac{d\sigma}{dp_T{}^2} \propto \left[1 + \left(\frac{35 \cdot \pi \cdot p_T}{256 \cdot \langle p_\mathrm{T} \rangle}\right)^2\right]^{-6}$$

and

$$\frac{d\sigma}{dx_F} \propto (1 - |x_F|)^c \ .$$

The average transverse momentum of $\langle p_\mathrm{T} \rangle = 1.29 \pm 0.01$ GeV/c is taken from a preliminary HERA-B analysis of the J/ψ sample recorded with a dilepton trigger [20]. The slight increase of the average transverse momentum with the mass of the nucleus is neglected. We take $c = 6.38 \pm 0.24$ as measured in proton-silicon collisions at 800 GeV/c [22]. The J/ψ's are generated without polarization. The influence of a possible J/ψ polarization within limits given by the experimental results [22-25] is taken into account as a systematic error. After the generation of the J/ψ the remaining energy is given as input to FRITIOF 7.02 [26] which generates the underlying event taking into account further interactions inside the nucleus.

The detector response is simulated with the GEANT 3.21 package [27]. Realistic detector efficiencies, readout noise and dead channels are taken into account. The simulated events are processed by the same reconstruction codes as the data. The total efficiencies, including track reconstruction as well as the influence of the selection cuts, are summarized in Table 4. The trigger efficiency for events containing a J/ψ meson is above 99%.

Target	$\epsilon(\mu^+\mu^-)$	$\epsilon(e^+e^-)$
C Below 1	0.337 ± 0.003	0.256 ± 0.003
C Inner 2	0.339 ± 0.004	0.261 ± 0.004
Ti Below 2	0.325 ± 0.003	0.247 ± 0.002
W Inner 1	0.317 ± 0.002	0.235 ± 0.002

Table 4
Total efficiency of reconstruction and selection cuts in the rapidity interval $-1.25 < y < +0.35$. The uncertainties quoted are the statistical uncertainties of the MC simulation.

6 Results

6.1 Combined cross sections per nucleus

The first step in determining the production cross sections is to combine, for each target material, the results of the two different final states. This is possible because the two measurements are statistically independent and compatible. The weighted average takes into account the statistical errors as well as those systematic errors which depend on the lepton species (contributions 1 - 2 of Sec. 6.2). The visible cross sections per nucleus, i.e. the cross sections measured in the rapidity interval of $-1.25 < y < +0.35$, are given by

$$\Delta\sigma_{pA}^{J/\psi} = \frac{N_i}{Br(J/\psi \to \ell^+\ell^-) \cdot \epsilon_i \cdot \mathcal{L}_i}$$

where

- N_i, ϵ_i and $\mathcal{L}_i$ are the measured J/ψ yield, the efficiency (Table 4) and the integrated luminosity (Table 1) for a particular target,
- Br is the branching fraction which is (5.88 ± 0.10) % for $J/\psi \to \mu^+\mu^-$ and (5.93 ± 0.10) % for $J/\psi \to \mathrm{e^+e^-}$ [28].

The combined cross sections $\Delta\sigma_{pA}^{J/\psi}$, summarized in Table 5, are almost independent of the assumptions made on the differential distributions (see Sec. 5).

However, for the total cross sections an extrapolation factor $1/f$ must be applied which depends on the shape of the rapidity distribution. This factor $f = 0.631 \pm 0.010$ is determined from the rapidity distribution of the J/ψ mesons generated in the Monte Carlo simulation.

The total cross sections obtained by extrapolation of the visible cross sections

$$\sigma_{pA}^{J/\psi} = \frac{\Delta\sigma_{pA}^{J/\psi}}{f}$$

are also given in Table 5.

Target	A	$\Delta\sigma_{pA}$ (μb)	σ_{pA} (μb)
carbon	12.011	$4.0 \pm 0.7 \pm 0.3$	$6.3 \pm 1.1 \pm 0.5$
titanium	47.867	$17. \pm 6. \pm 1.$	$27. \pm 9. \pm 2.$
tungsten	183.84	$75. \pm 11. \pm 5.$	$118. \pm 18. \pm 8.$

Table 5
Visible $\Delta\sigma_{pA}$ (in the rapidity interval $-1.25 < y < +0.35$) and total σ_{pA} J/ψ cross sections per nucleus of atomic weight A. The errors quoted indicate the statistical and systematic uncertainties, respectively.

6.2 Systematic Uncertainties

The total systematic uncertainty of the production cross sections is composed of the following contributions:

(1) Particle identification cuts are varied over a wide range and, for each set of cut values, the cross section is evaluated. The variation of the cross section corresponds to 2.5% for $J/\psi \to \mu^+\mu^-$ and 2.0% for $J/\psi \to e^+e^-$, respectively.
(2) Allowing for extreme variations of both signal shape and background parameterization, we estimate the rms uncertainty on signal counting by dividing the difference of the extreme values by $\sqrt{12}$ resulting in 2.5% for $J/\psi \to \mu^+\mu^-$ and 8% for $J/\psi \to e^+e^-$.
(3) The luminosity uncertainties of each data sample are shown in Table 1.
(4) The overall scaling error of the luminosity is 2.0% [17].
(5) The track reconstruction efficiency is tested separately for VDS and OTR using K_s^0 decays. One of the charged pions is reconstructed based on VDS (or OTR) and RICH/ECAL information only. Applying the same procedure to Monte Carlo data, we obtain an uncertainty of the track reconstruction efficiency of 1.5% per track.

(6) The uncertainty of the Monte Carlo production model within our kinematical range is 2.5%. This includes variations of the p_T shape as well as of the polarization parameter. Varying the exponent c of the x_F distribution within errors has negligible influence on our reconstruction efficiency. Reducing the exponent c from 6.38 to 5.0 corresponds to a 1% change in the efficiency.
(7) Each of the branching fractions for $J/\psi \to \mu^+\mu^-$ and $J/\psi \to \mathrm{e}^+\mathrm{e}^-$ has an uncertainty of 1.7% [28].
(8) The uncertainty on the extrapolation to the full rapidity range is determined by varying the exponent of the x_F parameterization within the errors to be 1.5%.
(9) Using $\sigma_{pA}^{J/\psi} = \sigma_{pN}^{J/\psi} \cdot A^{\alpha}$ as parameterization of the A-dependence, the uncertainty of $\alpha = 0.96 \pm 0.01$ [29] corresponds to a 3.6% uncertainty of the cross section per nucleon.

6.3 Cross sections per nucleon

As a last step, the results of the three data samples are combined to determine the cross section per nucleon $\sigma_{pN}^{J/\psi}$. The cross section for J/ψ production on a nuclear target of atomic weight A is parameterized as

$$\sigma_{pA}^{J/\psi} = \sigma_{pN}^{J/\psi} \cdot A^{\alpha}.$$

By fitting this expression to our data we can determine the cross section per nucleon. However, the limited statistics of our sample does not allow for a precise measurement of the A-dependence. Therefore we fix the parameter to the mid-rapidity measurement $\alpha = 0.96 \pm 0.01$ of E866 [29]. Fig. 5 demonstrates that our result is in good agreement with this assumption ($\chi^2/NDF = 1.5/2$). For this fit only the statistical and the relevant systematic uncertainties (1 - 3 of Sec. 6.2) are taken into account.

As a result we obtain

$$\sigma_{pN}^{J/\psi} = 663 \pm 74 \pm 46 \text{ nb/nucleon}$$

for the total J/ψ production cross section per nucleon. The systematic uncertainty quoted comprises all contributions described in Sec. 6.2.

The mid-rapidity cross section can be derived by applying a factor $\eta = 1.50 \pm 0.03$ which corrects for the difference between the differential cross section at $y = 0$ and the visible cross section, which is an average of the interval

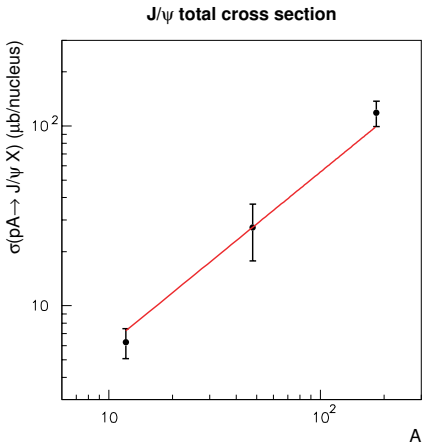

Figure 5. The total J/ψ cross section on nuclear targets C, Ti and W. The error bars indicate the statistical and systematic uncertainties 1 - 3 explained in Sec. 6.2. The line shows the result of the fit described in the text using $\alpha = 0.96$.

$-1.25 < y < +0.35$ with $\Delta y = 1.6$

$$\left.\frac{d\sigma_{pN}^{J/\psi}}{dy}\right|_{y=0} = \frac{\Delta\sigma_{pN}^{J/\psi}}{\Delta y} \cdot \eta = 392 \pm 44 \pm 27 \text{ nb/nucleon.}$$

7 Comparison with other results

Comparing our results to the measurements of previous experiments in proton-induced interactions requires correcting all results for the same branching fractions and A-dependence. All results shown in Fig. 6 are updated for the latest values of the branching fractions quoted in Sec. 6 and a target mass dependence assuming $\alpha = 0.96 \pm 0.01$. The systematic uncertainties are recalculated accordingly.

It is obvious that the experimental results are far from being consistent. Cross sections measured at nearby beam energies are not compatible when taking into account just the errors quoted by the experiments. Also shown on the figure is a fit to the published data on proton-induced J/ψ and $\psi(2S)$ production in the context of a next-to-leading order NRQCD calculation [50]. Several fits are performed with different subsets of measurements and different parton distribution functions (PDF). The best description of the data is obtained with the PDF MRST2002 [51].

At $\sqrt{s}$ =41.6 GeV, the fit gives a cross section of

$$\sigma_{\text{average}}^{J/\psi} = 502 \pm 44 \text{ nb/nucleon}$$

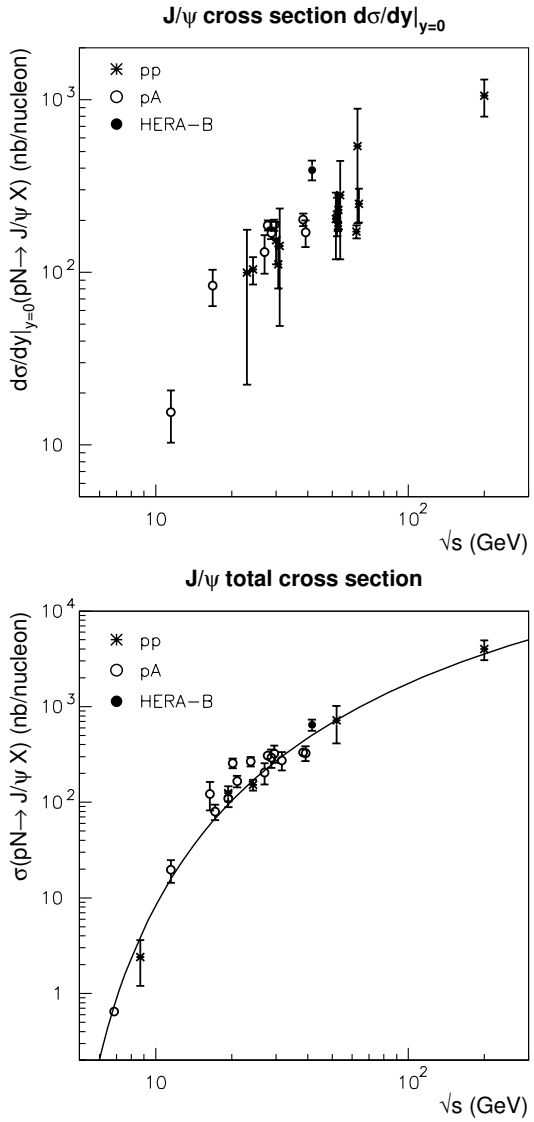

Figure 6. J/ψ production cross sections in proton-induced interactions [22-24, 30-47]. pp and pA measurements are indicated by different symbols. a) Differential cross section $d\sigma_{pN}/dy$ at y=0; b) total cross section σ_{pN} together with the fit described in the text.

which is in reasonable agreement with the result presented here. The error takes into account both fit uncertainties as well as systematics due to the parton distribution function. Details of the procedure together with tables of all experimental input used are the subject of a separate paper [52].

8 Summary

A data sample taken with a minimum bias trigger by the HERA-B experiment in interactions of 920 GeV/c protons with carbon, titanium and tungsten targets has been used to determine the production cross section of J/ψ mesons. In our data sample we find 100 ± 12 $J/\psi \to \mu^+\mu^-$ and 57 ± 13 $J/\psi \to \mathrm{e}^+\mathrm{e}^-$ candidates. After correcting for the efficiency of the selection criteria within the range in rapidity of $-1.25 < y < +0.35$ and combining both final states, we obtain the visible cross sections per nucleus within the detector acceptance. Using $\sigma_{pA}^{J/\psi} = \sigma_{pN}^{J/\psi} \cdot A^{0.96\pm0.01}$ to parameterize the A-dependence, and extrapolating this measurement to the full y range, the total production cross section per nucleon is

$$\sigma_{pN}^{J/\psi} = 663 \pm 74 \pm 46 \text{ nb/nucleon.}$$

For the cross section at mid-rapidity we obtain

$$\left.\frac{d\sigma_{pN}^{J/\psi}}{dy}\right|_{y=0} = 392 \pm 44 \pm 27 \text{ nb/nucleon.}$$

An NRQCD based fit of published results on J/ψ and $\psi(2S)$ production predicts $\sigma_{\text{average}}^{J/\psi} = 502 \pm 44$ nb/nucleon at 920 GeV/c, in reasonable agreement with this measurement.

Acknowledgments

We are grateful to the DESY laboratory and to the DESY accelerator group for their strong support since the conception of the HERA-B experiment. The HERA-B experiment would not have been possible without the enormous effort and commitment of our technical and administrative staff.

References

[1] J.J. Aubert et al., Phys. Rev. Lett. **33**, 1404 (1974).

[2] J.E. Augustin et al., Phys. Rev. Lett. **33**, 1406 (1974).

[3] F. Abe et al. (CDF collaboration), Phys. Rev. Lett. **79**, 572 (1997).

[4] G.T. Bodwin, E. Braaten and G. Lepage, Phys. Rev. D **51**, 1125 (1995); erratum *ibid.* D **55**, 5853 (1997).

[5] P. Cho and A. Leibovich, Phys. Rev. D **53**, 150 (1996).

[6] E. Braaten and S. Fleming, Phys. Rev. Lett. **74**, 3327 (1995).

[7] M. Beneke and I.Z. Rothstein, Phys. Rev. D **54**, 2005 (1996); erratum *ibid.* D **54**, 7082 (1996).

[8] J.F. Amundson et al., Phys. Lett. B **390**, 323 (1997).

[9] C. Brenner Mariotto, M.B. Gay Ducati and G. Ingelman, Eur. Phys. J. C **23**, 527 (2002).

[10] K. Ehret et al., Nucl. Instr. Meth. A **446**, 190 (2000).

[11] C. Bauer et al., Nucl. Instr. Meth. A **501**, 39 (2003).

[12] W. Gradl et al., Nucl. Instr. Meth. A **461**, 80 (2001).

[13] H. Albrecht et al., Nucl. Instr. Meth. A **541**, 610 (2005); arXiv/physics/0507048, DESY 05-99, submitted to Nucl. Instr. Meth. A.

[14] I. Ariño et al., Nucl. Instr. Meth. A **516**, 445 (2004).

[15] G. Avoni et al., Nucl. Instr. Meth. A **461**, 332 (2001).

[16] V. Eiges et al., Nucl. Instr. Meth. A **461**, 104 (2001).

[17] M. Bruschi, Luminosity determination at HERA-B, HERA-B note 05-011, to be published.

[18] I. Abt et al. (HERA-B collaboration), Improved measurement of the $b\bar{b}$ production cross section in 920 GeV fixed-target proton-nucleus collisions, Desy 05-233; submitted to Phys. Rev. D.

[19] A. Spiridonov, DESY report Desy-04-105 (2004).

[20] A. Zoccoli, Proc. of the International Conference on Hard and Electromagnetic Probes of High Energy Nuclear Collisions, Ericeira, Portugal, November 4-10, 2004, Eur. Phys. J. C **43**, 179 (2005).

[21] T. Sjostrand, Comp. Phys. Commun. **82**, 74 (1994).

[22] T. Alexopoulos et al. (E771 collaboration), Phys. Rev. D **55**, 3927 (1997).

[23] E.J. Siskind et al. (E595 collaboration), Phys. Rev. D **21**, 628 (1980).

[24] A. Gribushin et al. (E672/706 collaboration), Phys. Rev. D **62**, 012001 (2000).

[25] T.H. Chang et al. (E866 collaboration), Phys. Rev. Lett. **91**, 211801 (2003).

[26] H. Pi, Comp. Phys. Commun. **71**, 173 (1992).

[27] R. Brun et al., GEANT3, Internal Report CERN-DD/EE/84-1, CERN (1987).

[28] S. Eidelmann et al., Review of Particle Physics, Phys. Lett. B **592**, 1 (2004).

[29] M.J. Leitch et al. (E866 collaboration), Phys. Rev. Lett. **84**, 3256 (2000).

[30] A. Bamberger et al., Nucl. Phys. B **134**, 1 (1978).

[31] M.J. Corden et al. (WA39 collaboration), Phys. Lett. **98B**, 220 (1981).

[32] Yu.M. Antipov et al., Phys. Lett. **60B**, 309 (1976).

[33] K.J. Anderson et al. (E331 collaboration), Phys. Rev. Lett. **36**, 237 (1976); Phys. Rev. Lett. **37**, 799 (1976).

[34] J. Badier et al. (NA3 collaboration), Z. Phys. C **20**, 101 (1983).

[35] J.G. Branson et al. (E331 collaboration), Phys. Rev. Lett. **38**, 1331 (1977).

[36] K.J. Anderson et al. (E444 collaboration), Phys. Rev. Lett. **42**, 944 (1979).

[37] J.H. Cobb et al., Phys. Lett. **68B**, 101 (1977).

[38] L. Antoniazzi et al. (E705 collaboration), Phys. Rev. D **46**, 4828 (1992).

[39] C. Morel et al. (UA6 collaboration), Phys. Lett. B **252**, 505 (1990).

[40] H.D. Snyder et al. (E288 collaboration), Phys. Rev. Lett. **36**, 1415 (1976).

[41] M.C. Abreu et al. (NA51 collaboration), Phys. Lett. B **438**, 35 (1998).

[42] M.C. Abreu et al. (NA38 collaboration), Phys. Lett. B **444**, 516 (1998).

[43] B. Alessandro et al. (NA50 collaboration), Eur. Phys. J. C **33**, 31 (2004).

[44] C. Kourkoumelis et al., Phys. Lett. **91B**, 481 (1980).

[45] A.G. Clark et al., Nucl. Phys. B **142**, 29 (1978).

[46] M.H. Schub et al. (E789 collaboration), Phys. Rev. D **52**, 1307 (1995).

[47] E. Nagy et al., Phys. Lett. **60B**, 96 (1975).

[48] E. Amaldi et al., Lett. Nuo. Cim. **19**, 152 (1977).

[49] S.S. Adler et al. (PHENIX collaboration), Phys. Rev. Lett. **92**, 051802 (2004).

[50] F. Maltoni, hep-ph/0007003.

[51] A.D. Martin et al., Eur. Phys. J. **28**, 455 (2003).

[52] M. Bargiotti et al., Analysis of charmonium production at fixed-target experiments in the NRQCD approach, in preparation; Hera-B internal note 05-015.